Polish J. Chem., **78**, 1885–1892 (2004) **PHYSICAL CHEMISTRY**

Luminescence of Bismuth, Cerium and Terbium in Alkaline Earth Borates

by Y. Xie[1], S. Zhang[2] and Q. Zeng*[3]

[1]*Shekou Laboratory, Intertek Testing Services Shenzhen Ltd., 518067, P. R. China*
[2]*Department of Chemistry, Shaoguan College, 512005, P. R. China*
[3]*Key Laboratory of Rare Earth Chemistry and Physics, Changchun Institute of Applied Chemistry, Chinese Academy of Sciences, Changchun, 130022, P. R. China*

(Received November 24th, 2003; revised manuscript March 29th, 2004)

The luminescence of Bi^{3+}, Ce^{3+} and Tb^{3+}-activated BaB_8O_{13} and Sr-borates are studied. The emission peak of Ce^{3+} in alkaline earth borates shifts to higher energy side with decreasing ratio of SrO/B_2O_3. The energy transfer from Ce^{3+} to Tb^{3+} in BaB_8O_{13} is studied.

Key words: luminescence, alkaline earth borates, bismuth, rare earth ions

The luminescence of Bi^{3+} and Ce^{3+} has attracted attentions for many years not only as sensitizers but also as activators in various types of hosts under the consideration of its absorption of UV energy and shows widely varying emission characteristics in a long range from UV to red region [1–4]. For the Bi^{3+} ion, the ground state is $^1S_0$ and the excited states with 6s6p configuration are $^1P_1$ and ^3P, which can still be split into three sublevels $^3P_0$, $^3P_1$ and $^3P_2$ by the electron-lattice interaction (Jahn-Teller effect). In general, three bands ($^1S_0 \rightarrow {}^3P_2$, $^1S_0 \rightarrow {}^3P_1$ and $^1S_0 \rightarrow {}^1P_1$) are observed in the order of increasing energy in its excitation spectrum. This energy sequence is independent of Bi^{3+} surroundings, while the positions of these energy levels are strongly affected by the environmental changes, especially by the coordinated anions with Bi^{3+}. The $^1S_0 \rightarrow {}^3P_1$ transition is spin-forbidden but has reasonably high oscillator strength due to the mixing of the $^3P_1$ and $^1P_1$ levels and is no longer pure singlet and triplet levels, respectively. Since the probability of the $^3P_1 \rightarrow {}^1S_0$ transition is much higher than that of the $^3P_0 \rightarrow {}^1S_0$ transition, emissions between the $^3P_0$ and $^1S_0$ levels are generally not observed at room temperature [2].

The luminescence of Bi^{2+}, Ce^{3+} and Mn^{2+} in BaB_8O_{13} and SrB_4O_7 has been reported elsewhere [6,7]. It was found that the alkaline earth borates are good hosts for efficient luminescence. In this paper, we report on the luminescence of Bi^{3+}, Ce^{3+} and Tb^{3+} in BaB_8O_{13}, $Sr_3B_2O_6$, $Sr_2B_2O_5$, SrB_2O_4 and SrB_4O_7.

* To whom all correspondence should be addressed; e-mail: zqinghua@yahoo.com

EXPERIMENTAL

The samples of BaB_8O_{13}, $Sr_3B_2O_6$, $Sr_2B_2O_5$, SrB_2O_4 and SrB_4O_7 are prepared by stoichiometrical mixtures of analytical-grade barium carbonate, boric acid (3 mol% excess for compensation of its evaporation) and Bi_2O_3, CeO_2 and Tb_4O_7 as dopant. The dopant concentration is 2% of the corresponding cation ions. The mixture are preheated in air at 500°C for 2 hours, then reground and heated at 800–850°C for further 5 hours.

The structure is checked by a Rigaku D/MAX-IIB X-ray powder diffractometer, using CuKα radiation. Samples turn out to be single phase. Photoluminescence measurements are performed on a SPEX DM3000F spectrofluorometer equipped with 0.22 m SPEX 1680 double monochromators (resolution 0.1 nm) and a 450 W Xenon lamp as excitation source. The spectra are not corrected for the light output. All of the spectra are taken at room temperature.

RESULTS AND DISCUSSION

The luminescence of BaB_8O_{13}:Bi. The excitation and emission spectra of Bi^{3+} in BaB_8O_{13} are shown in Fig. 1. The BaB_8O_{13}:Bi^{3+} shows the luminescence from ultraviolet to visible range. Two maxima at 300 and 378 nm are observed in the excitation spectra, originating from the ground state $^1S_0$ to the excited $^3P_1$ state. In the emission spectrum, two broad bands with peaks at 385 and 420 nm and a long tail extending to 550 nm are obtained. These two bands are the emissions from the $^3P_1 \rightarrow {}^1S_0$ transitions. As it was reported, there are two crystallographic sites for cations in the host lattice, namely Ba^{2+} and B^{3+} [8], hence, these two emission and excitation bands should then be assigned to the Bi^{3+} ions in these two different sites. Due to the large different ionic radii between Bi^{3+} and B^{3+} ions, a serious structural distortion occurs and the amount of the substitution of Bi^{3+} on B^{3+} position is thus less than on Ba^{2+} sites, which results in weak emission intensity. Furthermore, the occupancy of Bi^{3+} on Ba^{2+} site causes a charge difference which would be compensated by the ionized vacancy or by the interstitial O^{2-}.

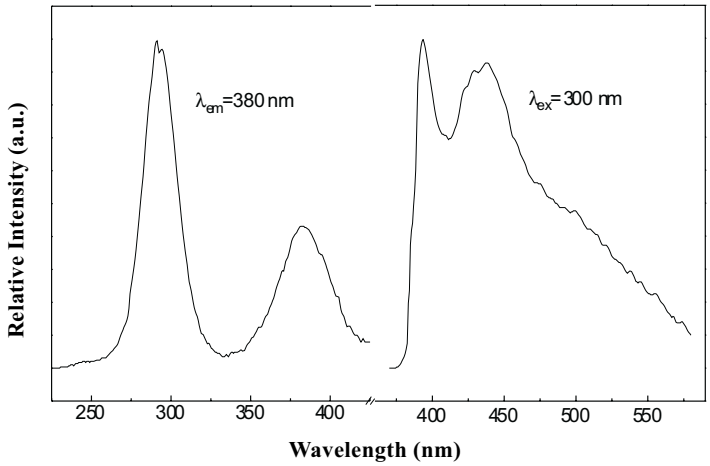

Figure 1. The excitation and emission spectra of Bi^{3+} in BaB_8O_{13}.

The excitation and emission positions of Bi^{3+} in different borates are given in Table 1. The emission peak of Bi^{3+} moves from compounds to compounds, but no reason is found to be responsible for these changes. It is likely due to the fact that the adiabatic potential energy surface of the relaxed $^3P_1$ level may contain two minima (A_T and A_X) due to the Jahn-Teller effect, from which the Bi^{3+} ion emits [4]. The long tail from 450 to 500 nm in the emission spectrum is ascribed to the Bi^{3+} ion in a borate glass or in a site with defect charge in view of the different valence between Ba^{2+} and Bi^{3+}. As in such sites, the lattice is "softer" than in the crystallographic sites. Due to the larger space available for Bi^{3+} in $Sr_3B_2O_6$ than in $Ca_3B_2O_6$, the Stokes shift is larger in former than in the later one [9], as shown in Table 1. However, one should note that the Stokes shift of Bi^{3+} in SrB_4O_7 is unusually large which indicates an off-center position of Bi^{3+} on the Si^{2+} sites since the Bi^{3+} favors an asymmetrical coordination due to the pseudo-Jahn-Teller effect [10,11]. It was found that the Stokes shift is related to the optical trap depth, *e.g.* the energy difference between the $^3P_1$ and $^3P_0$ level (about 400 cm^{-1}), and it is independent of the Bi^{3+} concentration. Smaller Stokes shift are often observed for smaller CN while larger Stokes shift for larger CN [3].

Table 1. The excitation and emission data of Bi^{3+} in alkalineearth borates.

Compounds	Structure	Excitation (nm)		Emission (nm)	Stokes shift	Ref.
		$^1S_0$-$^1P_1$	$^1S_0$-$^3P_1$	$^3P_1$-$^1S_0$	(cm^{-1})	
$Ca_2B_2O_5$	Mon.	216	293	357	6118	
$Ca_3B_2O_6$	Hex.	216	261, 282	350	8374	11
$Sr_3B_2O_6$	Hex.	217	271	364	9428	
SrB_4O_7	Orth.	217	241	450	15000	10
BaB_8O_{13}	Orth.		300, 378	380, 420	7000	this work

The luminescence of Tb^{3+} and energy transfer from Ce^{3+} to Tb^{3+} in BaB_8O_{13}. The luminescence of Tb^{3+} in BaB_8O_{13} shows its typical spectrum (Fig. 2). The sample emits green luminescence under UV excitation. In the emission spectrum, the lines at about 488, 547, 585 and 625 nm are ascribed to the characteristic transitions of $^5D_4 \rightarrow {}^7F_J$ (J = 6, 5, 4, 3). The emission spectrum does not change on varying of the excitation wavelength except the intensities. No emission from $^5D_3$ is found even at low concentration, which is likely quenched in the present sample. In generally, there are two main reasons to cause the quenching of $^5D_3$ transitions. The first one is the self-quenching, namely, the cross relaxation between $^5D_3$ and $^5D_4$ level [5]: $Tb^{3+}(^5D_3)+Tb^{3+}(^7F_6) \rightarrow Tb^{3+}(^5D_4)+Tb^{3+}(^7F_1)$. The second reason for the $^5D_3$ quenching is the multiphonon non-radiative relaxation [12]. It was found, that if the energy difference of $^5D_3$ and $^5D_4$ levels amounts five times of the highest-frequency phonon energies, the non-radiative relaxation easily occurs between these two energy levels [13]. In BaB_8O_{13}, the IR spectrum shows that the highest frequency of the vibration mode of the borate group is about 1400 cm^{-1} (asymmetric stretching mode of BO_3) [14]. The energy difference between $^5D_3$ and $^5D_4$ is about 5700 cm^{-1}, it can be

bridged by only four phonons. Therefore, due to the high energy phonons in the host lattice, the probability of non-radiative transition for the $^5D_3$ level to $^5D_4$ level is very high and no transition from $^5D_3$ level is found in BaB_8O_{13}:Tb^{3+}. Such non-radiative transition is also observed in other borates [15].

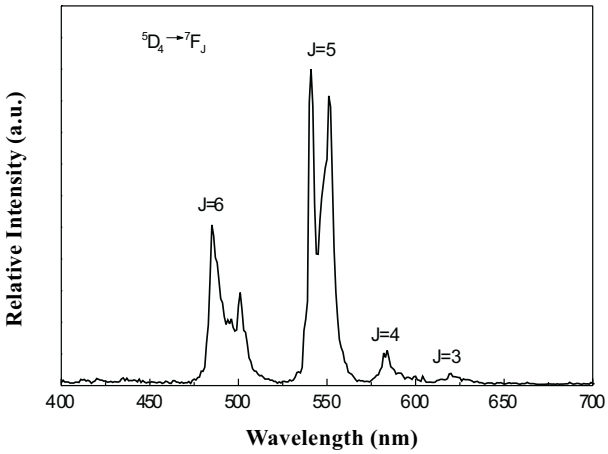

Figure 2. The emission spectrum of Tb^{3+} in BaB_8O_{13} under the excitation.

The energy transfer from Ce^{3+} to Tb^{3+}. The luminescence of Ce^{3+} in BaB_8O_{13} was reported in literature [6]. The broad emission band of Ce^{3+} in BaB_8O_{13} is at 350 nm which overlap the absorption band of Tb^{3+}. It is expected that energy transfer takes place between Ce^{3+} and Tb^{3+}. When the Ce^{3+} was excited at 312 nm, one can find a broad band at about 380 nm which is ascribed to the emission of Ce^{3+}. A series of line emissions at 488, 540, 590 and 615 nm can also be observed corresponding to the transitions of Tb^{3+} $^5D_4 \rightarrow ^7F_J$ (J = 3, 4, 5, 6). A broad excitation band at 270 and 310 nm can be seen when monitoring the emission of Tb^{3+} at 547 nm. Thus it is concluded that the energy transfer between Ce^{3+} and Tb^{3+} occurs. The emission intensity ratio of Ce^{3+} to Tb^{3+} is about 1.3:1. The transfer efficiency η_T can be calculated by [16]:

$$\eta_T = I - (\eta/\eta_0) = 1 - (I_d/I_{do}) \quad (1)$$

Where I_d, I_{do} is the luminescent intensity of the donor in the presence and absence, respectively, of the acceptor for the same donor concentration. The above equation is obtained, assuming that the number of phonons absorbed by the donor ions for a given phonon flux is the same in the presence or absence of the acceptor ions. In our case, we obtained the energy transfer efficiency $\eta_T \approx 60\%$. Therefore, the energy transfer from Ce^{3+} to Tb^{3+} is uncompleted and inefficient. Here the diffusion process for Ce^{3+}-Ce^{3+} should also be taken into the consideration. Figs. 3 and 4 depict the dependence of the luminescent intensity of Ce^{3+} and Tb^{3+} as a function of Tb^{3+} concentration. With increasing Tb^{3+} concentration, the intensity of Ce^{3+} decreases and that of Tb^{3+} increases.

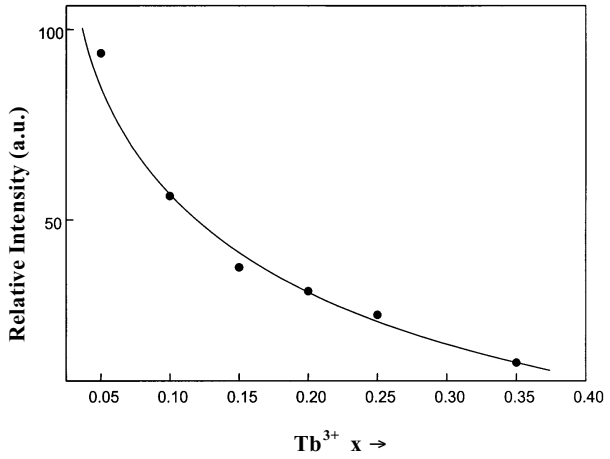

Figure 3. The dependence of the emission intensity of Ce^{3+} as a function of Tb^{3+} concentration in $Ba_{0.95-x}Ce_{0.05}Tb_xB_{7.95-x}Mg_{0.05+x}O_{13}$.

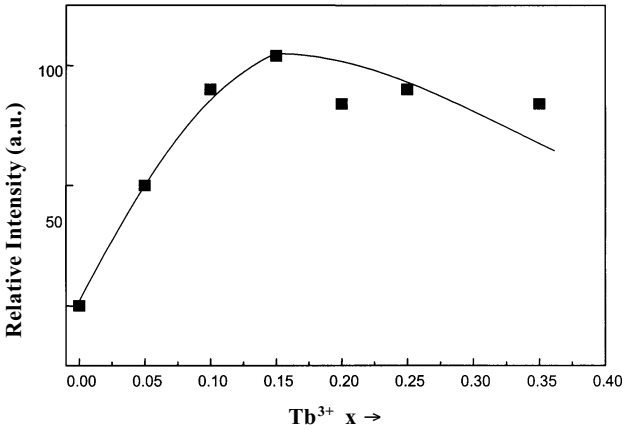

Figure 4. The dependence of the emission intensity of Tb^{3+} as a function of Tb^{3+} concentration in $Ba_{0.95-x}Ce_{0.05}Tb_xB_{7.95-x}Mg_{0.05+x}O_{13}$.

The energy transfer mechanism for Ce^{3+} to Tb^{3+} in BaB_8O_{13} can be described by the so-called discrete model and the energy can be transferred to the fourth shell. The luminescent efficiency of Ce^{3+} is given by [17]:

$$\eta_{Ce} = \eta_{Ce+Tb} \{(1-x-y)^5(1-y)+x(1-x-y)^8(1-y)^4+(1-(1-y)^4)(1-x-y)^8(1-y)^4\} \quad (2)$$

Where x is the concentration of Ce^{3+} and y the concentration of Tb^{3+}, η_{Ce} and η_{Ce+Tb} is the luminescent efficiency of Ce^{3+} and Ce^{3+}+Tb^{3+}. The experimental and calculation results from Eq. (2) are shown in Fig. 5.

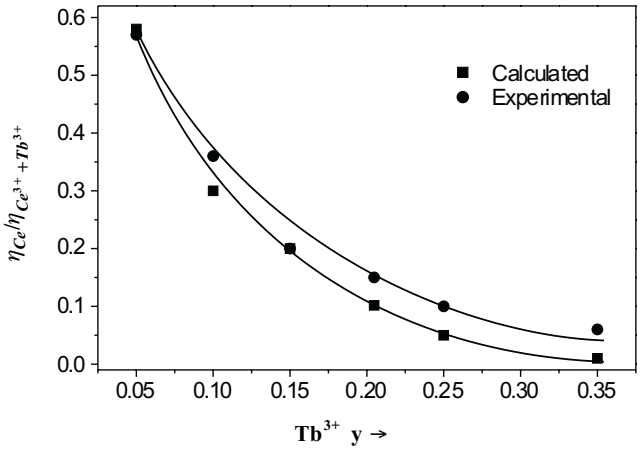

Figure 5. The variation of luminescence efficiency ratio η_{Ce}/η_{Ce+Tb} in $Ba_{0.95-x}Ce_{0.05}Tb_xB_{7.95-x}Mg_{0.05+x}O_{13}$.

It is deduced that the experimental results are in good agreement with the calculations at low concentrations of Tb^{3+} but a small deviation appears at high concentration. This is due to the fact that the body color of the compound is grayish at high concentration of Tb^{3+} and the samples may also contain some Tb^{4+} ions which do not luminance.

The luminescence of $Sr_3B_2O_6:Ce^{3+}$, $Sr_2B_2O_5:Ce^{3+}$ and $SrB_2O_4:Ce^{3+}$. The luminescence of Ce^{3+}-doped $Sr_3B_2O_6$, $Sr_2B_2O_5$ and SrB_2O_4 are studied. Here only the spectra of $Sr_3B_2O_6:Ce^{3+}$ are shown in Fig. 6. The excitation spectrum shows well-separated bands with maxima at 285 and 345 nm which are ascribed to the transitions from the ground state to the crystal-field components of the 5d excited states.

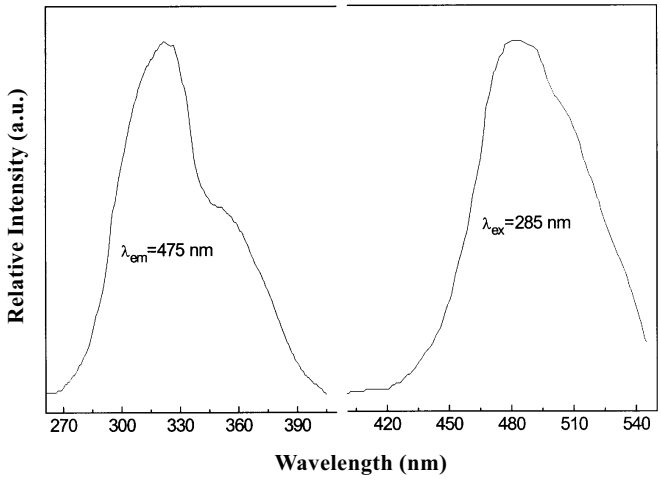

Figure 6. The excitation and emission spectra of Ce^{3+} in $Sr_3B_2O_6$.

The emission band consists of a broad band with a maximum at 475 nm, which is ascribed to the transition from the 5d level to the ground state with Stokes shift about 7930 cm^{-1}. Our results are different from those in literature [19] in which two emission bands at about 395 and 420 nm and the excitation bands at 250, 280 and 355 nm were reported with the Stokes shift about 2852 cm^{-1}. The difference may be explained by the fact that since our sample is prepared in air, the luminescence of vacancy-association Ce^{3+}-O^{2-} pairs is predominated, as mentioned above, which results in a more intense emission at long wavelength due to the higher covalency. The data for the excitation and emission spectra of Ce^{3+} doped Sr-borates are summarized in Table 2.

Table 2. The excitation and emission data of Ce^{3+} in alkaline earth borates.

MO/B_2O_3	Compounds	Excitation (nm)	Emission (nm)	Stokes shift (cm^{-1})	Ref.
3/1	$Ca_3B_2O_6$	289, 358	392, 421	2200	18
3/1	$Sr_3B_2O_6$	250, 280, 355	395, 420	2852	19
1/2	SrB_4O_7	207, 220	293, 314	1600	20
3/1	$Sr_3B_2O_6$	285, 345	475	7930	this work
2/1	$Sr_2B_2O_5$	268, 318, 38	387, 395	3746	this work
1/1	SrB_2O_4	267, 329, 340	370	2385	this work
1/2	SrB_4O_7	246, 279, 291	312, 365	2312	this work

From Table 2, one can observe that the emission peak of Ce^{3+} shifts toward higher energy side and the Stokes shift decreases with decreasing SrO/B_2O_3 ratio which results in "softer" lattice. The available space for Ce^{3+} also increases and the covalency of Ce^{3+}-O^{2-} increases. Hence the Stokes shift increases in the sequence of SrB_4O_7, SrB_2O_4, $Sr_2B_2O_5$ and $Sr_3B_2O_6$. It was reported that SrB_4O_7 is a very rigid host lattice that can restrict the relaxation of the excited states and results in small Stokes shift [21].

The excitation position of Ce^{3+} in $Sr_3B_2O_6$ is at the lowest energy side, as shown in Table 2, due to its strong crystal effect [18]. The crystal structure of this borate can be considered as anticorundum, *i.e*. a hexagonal close-packing of Sr^{2+} ions in which the borate groups occupy the octahedral sites [22]. The resulting Sr^{2+} coordination is complicated. It consists of eight oxygen ions and has a two-fold axis. Four of these oxygen ions belong to bidentate borate group, whereas the other four oxygen ions belong to monodentate borate groups. The monodentate borate groups are on opposite sides of the coordinating polyhedron. This may be the origin of the strong crystal-field component which shifts the 5d level of Ce^{3+} in $Sr_3B_2O_6$ to lower energy side.

CONCLUSIONS

Bi^{3+} in BaB_8O_{13} shows efficient emission which originates from the $^3P_1 \rightarrow {}^1S_0$ transition at room temperature. Two crystallographic sites for Bi^{3+} in the host lattice are available. The Tb^{3+} ions in BaB_8O_{13} show emission spectra of the $^5D_4 \rightarrow {}^7F_J$ (J = 6, 5, 4, 3) transitions but no transition from the $^5D_4$ to ^7F_J levels is observed due to the cross-relaxation and multiphonon non-radiative relaxation between the $^5D_3$ and $^5D_4$ levels. The luminescence of co-doped Ce^{3+} and Tb^{3+} in BaB_8O_{13} shows that the energy transfer *via* discrete mechanism takes place inefficiently. The emission of Ce^{3+} shifts to higher energy side and the Stokes shift decreases with decreasing ratio of SrO/B_2O_3 due to the stiffness of the host lattice.

REFERENCES

1. Blasse G. and Bril A., *J. Chem. Phys*., **48**, 217 (1968).
2. Sommerdijk J., Verstegen J. and Bril A., *Philips Res. Rep.*, **9**, 517 (1974).
3. Blasse G. and Van de Steen A., *Solid State Commun*., **31**, 993 (1979).
4. Fukuda A., *Phys. Rev.*, **B1**, 4161 (1970).
5. Blasse G., *Rev. Inorg. Chem.*, **5**, 319 (1983).
6. Zeng Q., Pei Z., Wang S. and Su Q., *Chin. J. Chem.*, **17**, 454 (1999).
7. Zeng Q., Zhang T., Pei Z. and Su Q., *J. Mater. Sci. Tech.*, **15**, 281 (1999).
8. Zeng Q., Pei Z., Su Q. and Lu S., *J. Lumin.*, **82**, 241 (1999).
9. Wolfert A., Oomen E. and Blasse G., *J. Solid State Chem.*, **59**, 280 (1985).
10. Blasse G., Meijerink A., Nomes M. and Zuidama J., *J. Phys. Chem. Solids*, **55**, 171 (1994).
11. Pei Z., Su Q. and Zhang J., *Solid State Commun*., **86**, 377 (1993).
12. Blasse G. and Sabbatini N., *Mater. Chem. Phys*., **16**, 237 (1987).
13. Blasse G., *Prog. Solid State Chem*., **18**, 79 (1988).
14. Weir C.E. and Schroedder R.A., *J. Res. NBS*., **68A(5)**, 465 (1964).
15. Fouassier C., Saubat B. and Hangmuller P., *J. Lumin.*, **23**, 405 (1981).
16. Parent C., Bochu P., Le Flem G., Hagenmuller P., Boucet J. and Gaume-Mahn F., *J. Phys. Chem. Solids*, **45**, 39 (1984).
17. Stevels A.L.N., *J. Lumin.*, **20**, 99 (1979).
18. Schipper W., Van der Voort D., Van de Berg P., Vroon Z. and Blasse G., *Mater. Chem. Phys.*, **33**, 311 (1993).
19. Koskentalo T., Niisto L. and Leskela M., *J. Less-Comm. Metals*, **112**, 67 (1985).
20. Leskela M., Kostentalo T. and Blasse G., *J. Solid State Chem.*, **59**, 272 (1985).
21. Blasse G., Dirksen G. and Meijerink A., *Chem. Phys. Lett.*, **167**, 41 (1990).
22. Vegas A., *Acta Cryst.*, **C41**, 1689 (1985).